Int. J. Electrochem. Sci., 12 **(2017)** 1118 – 1129, doi: 10.20964/2017.02.32

International Journal of
ELECTROCHEMICAL
SCIENCE
www.electrochemsci.org

$CoSe_2$ Nanoparticles as Anode for Lithium Ion Battery

Wanzheng Lu, Mingzhe Xue[*]*, Xiaolan Chen and Chen Chen*

Clean Energy Automotive Engineering Center, School of Automotive Studies, Tongji University, Shanghai 201804, China
[*]E-mail: heroxmz@hotmail.com, mzxue@tongji.edu.cn

Received: 15 November 2016 / *Accepted:* 12 December 2016 / *Published:* 30 December 2016

Orthorhombic $CoSe_2$ nanoparticles were synthesized via a facile one-step hydrothermal approach. The size, morphology, as well as phase structure were characterized by scanning electron microscopy (SEM) and powder X-ray diffraction (XRD). It was confirmed that $CoSe_2$/Li battery cycled between 2.5 V and 0 V was more appropriate than between 3.0 V and 0 V. And the initial discharge capacity was 975.9 mAh g^{-1} at a current density of 100 mA g^{-1}, while it increased after about 90 cycles, and even exceeded theoretical discharge capacity (494.4 mAh g^{-1}) after about 485 cycles due to the activating reactions and the electric double layer effect. Electrochemical mechanism of $CoSe_2$ as anode for lithium ion battery was verified by cyclic voltammetry (CV) and electrochemical impedance spectroscopy (EIS). It showed that solid electrolyte interface (SEI) started to be formed at 1.4 V in the first discharge process. SEI-film resistance (R_{SEI}), electron-transfer resistance (R_e), and charge-transfer resistance (R_{ct}) played the key part in the first discharge process of lithium intercalation respectively.

Keywords: $CoSe_2$ nanoparticles; Anode; Lithium ion battery; Electrochemical mechanism; Solid electrolyte interface

1. INTRODUCTION

In 2000, P. Poizot et al. reported the mechanism of Li^+ intercalating and deintercalating the transition metal oxides in Nature [1]. Before long, research on compounds based on transition metals (Co, Ni, Cu, Fe, Mo, etc.) has become a current research focus. And transition metal related compounds are regarded as promising electrode materials for the next generation lithium ion battery [2-6]. Selenium, element from the same group as oxygen, has lower electronegativity, which makes transition metal selenides the potential electrode material for lithium ion battery. What’s more, compared with transition metal oxides, transition metal selenides have higher bulk density, lower volume effect, better reversibility and rate performance. Theoretically, lithium ion battery with transition metal selenides anode is supposed to exhibit excellent electrochemical properties.

Current researches about transition metal selenide for lithium ion batteries mainly focus on $CoSe_2$ [7], $NiSe_x$ (x=1,2) [8-10], $MoSe_x$ (x=1,2) [11-13], MnSe [14,15], $SnSe_x$ (x=1,2) [16-24], FeSe [25,26], GeSe [24], Sb_2Se_3 [27,28], ZnSe [29-31], Ga_2Se_3 [32,33] and Bi_2Se_3 [34-36].

Compared with other transition metal selenides, $CoSe_2$ could be easily obtained by hydrothermal and solvothermal methods [37-42]. $CoSe_2$, as anode material for lithium ion battery exhibits high theoretical capacity (up to 494.4 mAh g^{-1}), theoretically, for 1 mol $CoSe_2$ could react with 4 mol Li^+ [7,9]. Besides that, when reacting with Li^+, Co/Li_2Se interface could store extra charges in analogy to capacitor [43,44], resulting in better capacity and rate performance. The lasted report on $CoSe_2$ for lithium ion battery indicated the discharge capacity increased after about some cycles and even graphene/cobalt selenide (rGO/$CoSe_2$) composite exceeded the theoretical value [7]. Thus, $CoSe_2$ is considered to be a promising electrode material for lithium ion battery with various potential applications. In this work, $CoSe_2$ nanoparticles were synthesized via a facile one-step hydrothermal approach, and $CoSe_2$ as anode for lithium ion battery cycled between 2.5 V and 0 V (vs. Li/Li^+) exhibited excellent electrochemical performance. And the capacity increased after about 90 cycles, and even exceeded theoretical discharge capacity (494.4 mAh g^{-1}) after about 485 cycles, which was similar to the previous report [7]. The mechanism of intercalation/deintercalation in the first discharge process was firstly illustrated via CV and EIS in detail in this paper. And SEI-film was formed at the interface of anode/electrolyte when polarization potential decreases from 1.4 V to 0.9 V. It was indicated that the generation of the SEI-film make a difference to electrolyte resistance (R_s), and it also was revealed that electron-transfer resistance (R_e), and charge-transfer resistance (R_{ct}) rather than SEI-film resistance (R_{SEI}) played the main role in the first discharge process of lithium intercalation.

2. EXPERIMENTAL

2.1 The preparation of $CoSe_2$ nanoparticles

The typical preparation process followed the following steps [37,41]. I solution: 8.0 g sodium hydroxide (NaOH) was completely dissolved in 60.0 mL deionized water. Then the solution was heated to 70-90 °C in silicone bath. 0.64 g selenium powder was added into the solution with magnetic stirring slowly. Keep stirring for 2 hours, selenium was totally dissolved and the solution turned dark. II solution: 1.8612 g ethylenediaminetetraacetic acid disodium salt (EDTA-2Na) was completely dissolved in 20 mL deionized water with gentle heat and magnetic stirring to make a even solution. Then 0.96 g cobalt chloride ($CoCl_2{\cdot}6H_2O$) was added slowly and the solution turn red. Then II solution was gently poured into I solution and kept stirring at 60 °C in silicone bath for 2 hours. The mixture was transferred to 100 ml Teflon vessel. After that, the vessel was put into an autoclave preheated to 180 °C. After reacting for 24 hours, the Teflon vessel was taken out and cooled to room temperature naturally. It was found there were a mass of the black products in Teflon vessel. The black products were washed by deionized water for several times until the Cl^- was clearly washed.

2.2 Characterizations

The morphology and size of the products were characterized by scanning electron microscopy (SEM, FEI SIRION 200/INCA, OXFORD). The crystal structure and microstructure were characterized by X-ray diffraction measurement (XRD, Rigaku DLMAX-2200).

2.3 Electrochemical tests

The electrochemical properties of the $CoSe_2$ electrodes were tested using coin-type half cells (CR 2032) which was assembled under an argon-filled glovebox. A working electrode was prepared by mixing the 80 wt% $CoSe_2$, 10 wt% super P and 10 wt% polyvinylidene fluoride (PVDF) in Nmethyl-2-pyrrolidinone (NMP). And 1.0 mol L^{-1} $LiPF_6$/EC+DEC+DMC (1:1:1, V/V/V) was applied as electrolyte. cyclic voltammetry test was perfomed on electrochemical workstation (CHI660D, Shanghai Chenhua Instrument Factory) by the negative scanning with a scan rate of 0.5 mV s^{-1}, and the voltage range was from 2.60 V to 0 V (vs. Li/Li^+)., EIS was tested from high frequency (10^5 Hz) to low frequency (0.01 Hz) at series of polarization potentials using electrochemical workstation (CHI660D, Shanghai Chenhua Instrument Factory).

3. RESULTS AND DISCUSSION

XRD pattern of the as-synthesized product is shown in Fig. 1. The diffraction peaks can be indexed to orthorhombic structure of pure $CoSe_2$ (JCPDS No. 53-0449).

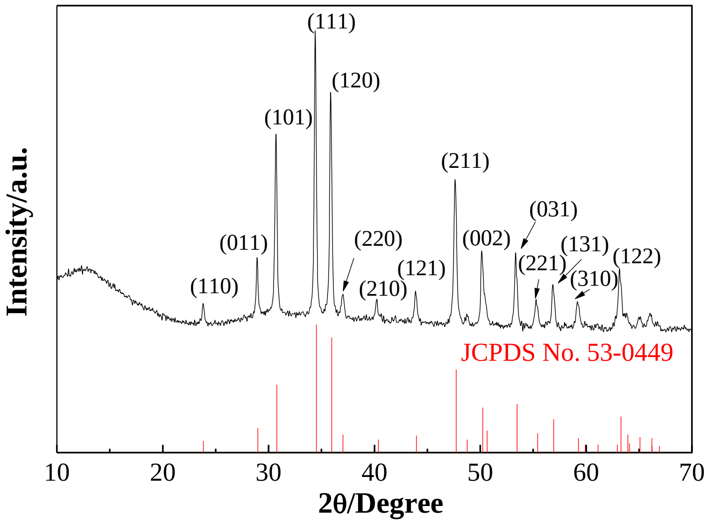

Figure 1. XRD pattern of as-synthesized product

The morphologies of the as-synthesized $CoSe_2$ are characterized by SEM. Fig. 2A exhibits regular particles with size of 100 nm on average. Particles agglomerate into regular spherical shape with size about 1 μm as shown in Fig. 2B.

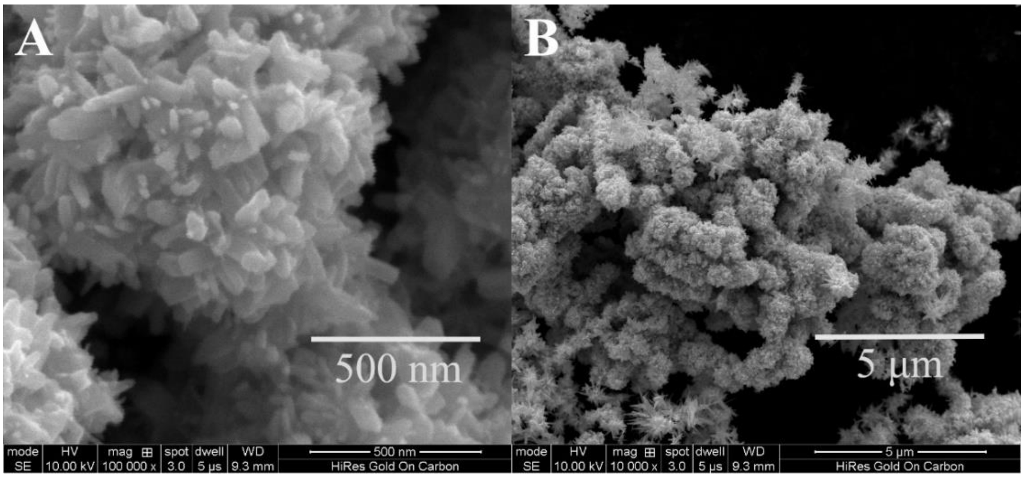

Figure 2. SEM images of as-synthesized $CoSe_2$ nanoparticles: (A) morphology at high magnification; (B) morphology at low magnification

It was reported the charge-discharge end voltage at constant current of $CoSe_2$/Li battery was supposed to be 3.0 V/0 V [7], but a new testing voltage range was applied in this work. Theoretically, a high charge end voltage might result in structural distortion of electrode material, directly causing the decrease of capacity. Besides, it has been reported that capacity of transition metal selenide for lithium ion battery could die dramatically. Thus it is commonly composited with carbon material. And, carbon/Li battery was usually cycled between 2.0 V and 0 V. As a result, a series of tests were applied to figure out the most appropriate voltage range in this work.

Cycling performances of $CoSe_2$ and $CoSe_2$@Carbon (the carbon is purchased in commerce and its content in the composites is estimated to be approximately 20.0 wt%) under a series of charge-discharge end voltage at 100 mA g^{-1} were shown in Fig.3A and Fig.3B respectively. The result shows that capacity keeps more steady when cycled between 2.5 and 0 V (vs. Li/Li^+). This may be caused by two main factors. Firstly, high charging voltage damaged the electrode material structure causing the decrease of reversible capacity. And secondly, carbon as anode material, performs better under lower potential.

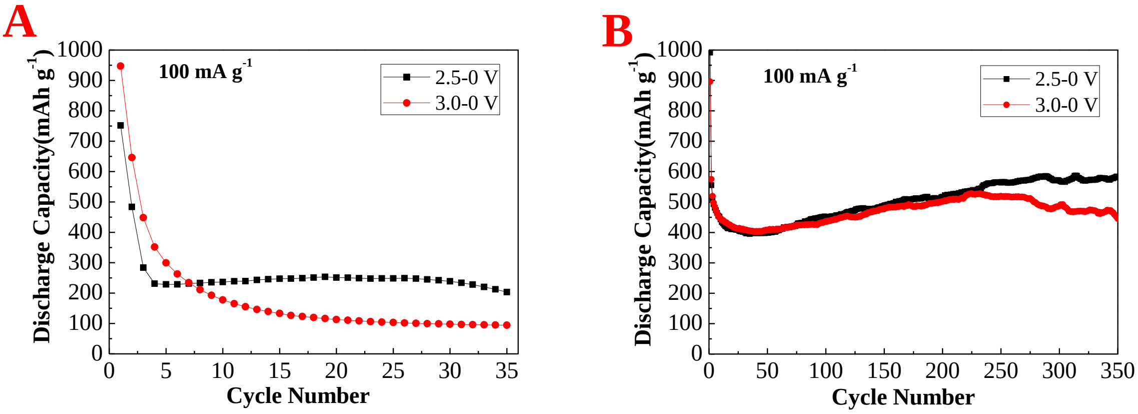

Figure 3. Cycling performances under a series of charge-discharge end voltage at 100 mA g^{-1}: (A) $CoSe_2$; (B) $CoSe_2$@Carbon

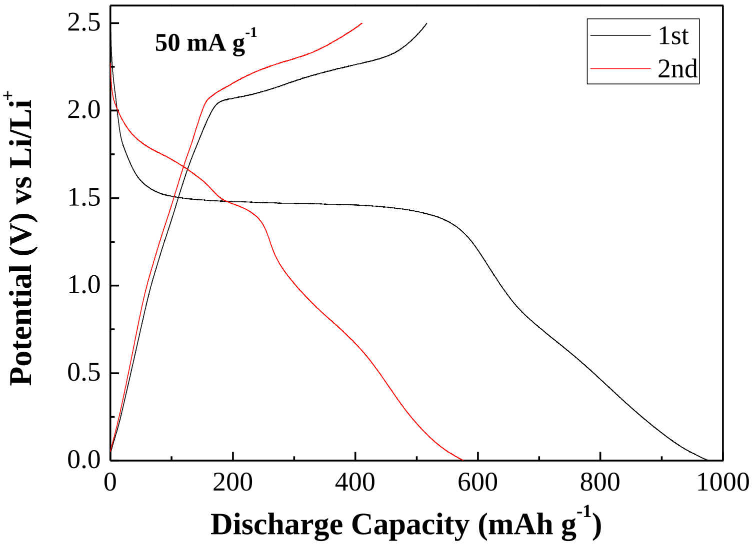

Figure 4. Galvanostatic charge-discharge curve of $CoSe_2$ cycled between 2.5 V and 0 V at 50 mA g^{-1}

Fig. 4 exhibits a discharge voltage plateau at about 1.5 V at the 1st cycle, but it disappears after the 2nd cycle. The initial discharge capacity at 50 mA g^{-1} is 975.9 mAh g^{-1}, and the figure keeps at 576.3 mAh g^{-1} at the 2nd cycle; the initial charge capacity is 516.9 mAh g^{-1}. Thus, 59.1% of the capacity maintained and 53.0% of coulombic efficiency were figured out. The formation of SEI-film and the accumulation of CoSe, Li_2Se and Co inside electrode cause the irreversible capacity. Some similar anode materials were listed in Table 1 and were compared with the $CoSe_2$ nanoparticles prepared in this work.

Table 1. Comparison between $CoSe_2$ nanoparticles and similar anode materials in literature

Anode material	Charge-discharge current density (mA g^{-1})	Charge-discharge end voltage	Initial discharge capacity (mAh g^{-1})	Initial charge capacity (mAh g^{-1})	References
$CoSe_2$ nanoparticles	50	2.5-0 V	975.9	516.9	This work
$NiSe_2$ thin film	50	3.0-1.0 V	468.5	460.3	[9]
α-MnSe nanocubes	100	3.0-0 V	790.0	401.0	[14]
SnSe nanosheets	50	3.0-0.01 V	1009.0	417.0	[17]
α-FeSe nanoparticles	40	3.0-1.0 V	390.0	350.0	[25]
ZnSe spheres	100	3.0-0.01 V	960.0	530.0	[31]
Bi_2Se_3 microrods	50	3.0-0.01 V	870.0	703.0	[35]

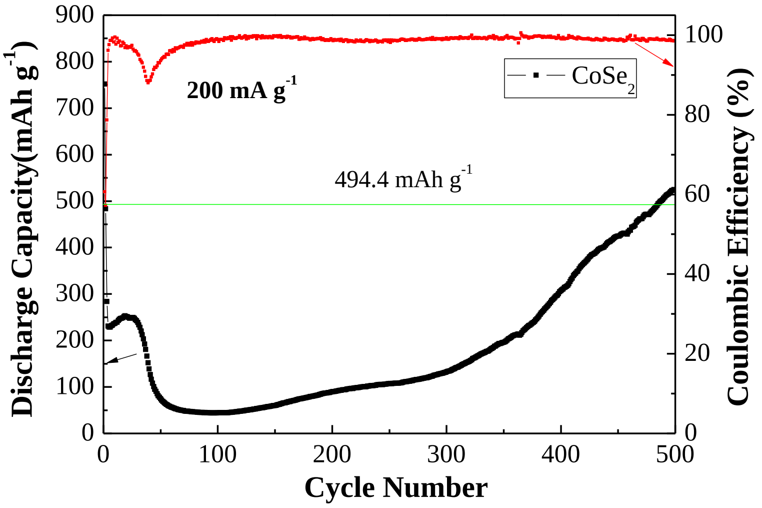

Figure 5. Cycling performances and coulombic efficiency of $CoSe_2$ cycled between 2.5 V and 0 Vat 250 mA g^{-1}

Fig. 5 shows the capacity of $CoSe_2$ at 250 mA g^{-1} keeps steady in the first 30 cycles, but it decrease continuously until the 90th cycle. From the 90th cycle, the discharge capacity keeps going upward and finally exceeds the theoretical value (494.4 mAh g^{-1}) after about 485 cycles.

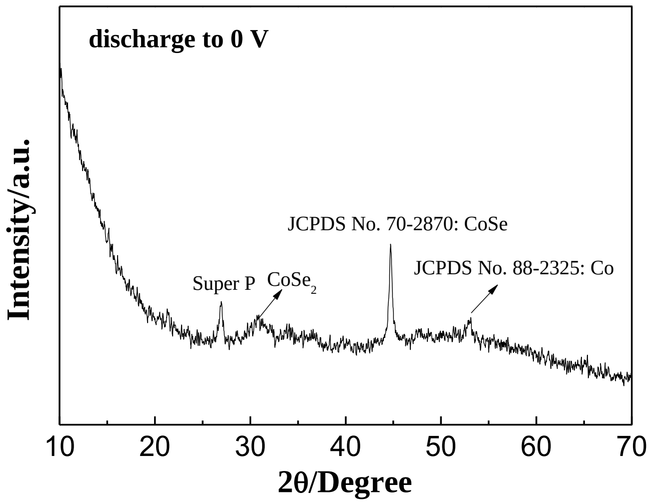

Figure 6. XRD pattern of working electrode material when discharged to 0 V

The reasons for this phenomenon could be revealed through some previous reports [7,9] and some testings. Fig. 6 shows XRD pattern of working electrode material when discharged to 0 V; the diffraction peak of CoSe was sharp indexed to JCPDS No. 70-2870 and the diffraction peak of Co was indexed to JCPDS No. 88-2325. Some relevant reports [7,9,45] indicated that two reactions took place in the battery during the cycle, (I) at the high potential and (II) at the low potential. Reaction (I) and (II) could be confirmed through Fig.6 in our work. Only when the accumulation of $CoSe+Li_2Se$

reaches a certain amount (cycled about 90 cycles), can the $CoSe_2$ electrode system be kinetically activated to generate more defects and active sites [7,46,47] increasingly. Besides, there is the electric double layer effect[43] in the Co/Li_2Se interface storing extra charges [44]. Fig.7 shows the two-dimensional pattern of interfacial charge storage lithium of Co/Li_2Se (electric double layer effect).

(I) $2Li^+ + 2e^- + CoSe_2 \leftrightarrow CoSe + Li_2Se$
(II) $2Li^+ + 2e^- + CoSe \leftrightarrow Co + Li_2Se$

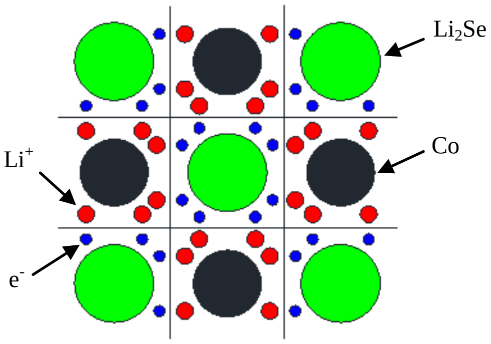

Figure 7. Interfacial charge storage lithium of Co/Li_2Se

CV curves of $CoSe_2$ at 0.5 mV s^{-1} from 2.60 V to 0 V (vs. Li/Li^+) is shown in Fig. 8. The peaks at 1.267 V and 0.524 V represent reduction peaks. The peaks at 2.194 V and 2.461 V represent oxidation peaks. The reduction-oxidation couple (1.267 V and 2.461 V) correspond to the formation of SEI and reaction (I) and the other reduction-oxidation couple (0.524 V and 2.194 V) correspond to reaction (II). The peak at 1.267 V is sharper than that at 0.524 V indicating that Li^+ consumption caused by the formation of SEI and reaction (I), is much more than that of reaction (I). The oxidation peaks are not as sharp as reduction peaks, indicating that reaction (I) and reaction (II) cause the accumulation of CoSe, Li_2Se and Co inside electrode, generating the irreversible capacity.

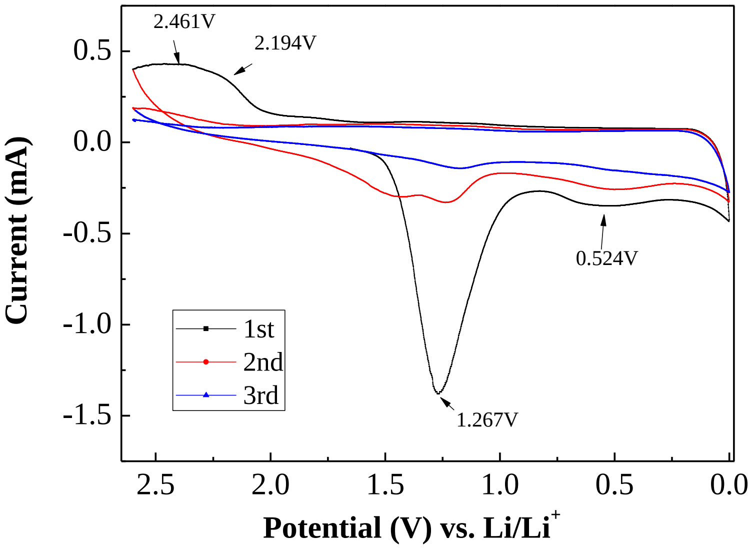

Figure 8. The first there consecutive CV curves of $CoSe_2$ at 0.5 mV s^{-1} from 2.60 V to 0 V (vs. Li/Li^+)

Nyquist plots of the $CoSe_2$ electrode at various polarization potentials (vs. Li/Li^+) in the first discharge process are shown in Fig. 9A, Fig. 9B, Fig. 9C, Fig. 9D and Fig. 9E. When polarization potential decreases to 1.4 V, there are four time constants, three arcs and one line. The first arc in the high frequency region (68120-122.1 Hz) represents the resistance and impedance contributed by SEI. The second arc in the middle frequency region (0.3831-0.02154 Hz) represents electron-transfer resistance and impedance. And the third arc in the low frequency region (0.01778-0.01 Hz) represents charge-transfer resistance and impedance of Li^+ inside $CoSe_2$ electrode. The line in the super low frequency region represents the diffusion impedance of Li^+ in the whole system.

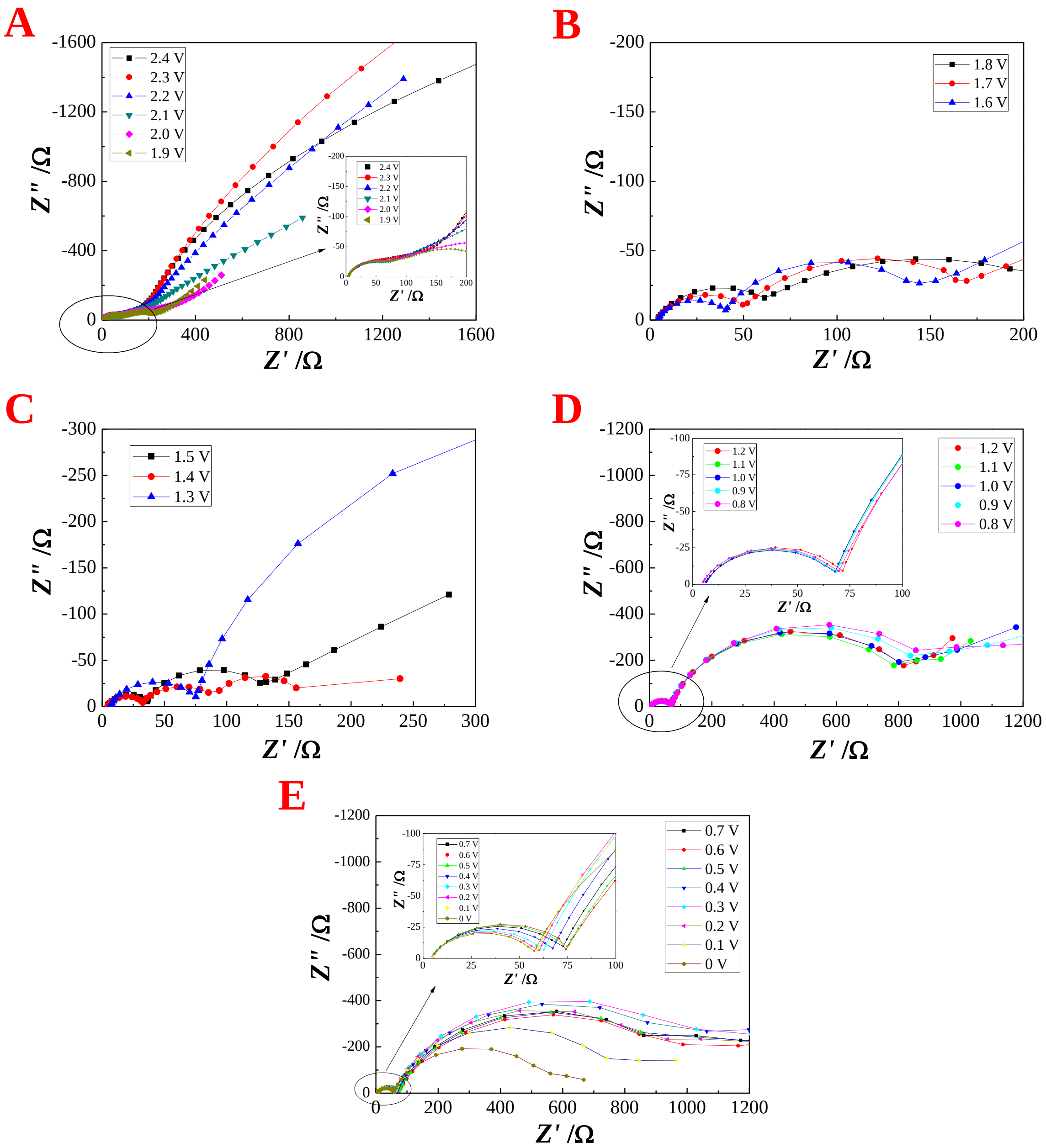

Figure 9. Nyquist plots of $CoSe_2$ electrode at various polarization potentials (vs. Li/Li^+) in the first discharge process: (A) 2.4-1.9 V; (B) 1.8-1.6 V; (C) 1.5-1.3 V; (D) 1.2-0.8 V; (E) 0.7-0 V

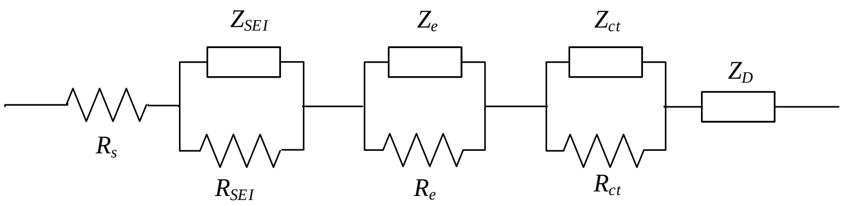

Figure 10. Equivalent circuit proposed for $CoSe_2$ electrode in first discharge process

Equivalent circuit which was proposed for $CoSe_2$ electrode in the first discharge process is shown in Fig. 10. R_s, R_{SEI}, R_e and R_{ct} respectively represent electrolyte resistance, SEI-film resistance, electron-transfer resistance and charge-transfer resistance. Z_{SEI}, Z_e, Z_{ct} and Z_D respectively represented SEI-film impedance, electron-transfer impedance, charge-transfer impedance and the diffusion impedance of Li^+ in the whole system [48,49].

Fig. 11A exhibits variations of R_s with the electrode polarization potentials for $CoSe_2$ in the first discharge process. R_s keeps steady at about 4.200 Ω, when polarization potential decrease from 2.4 V to 1.4 V. However, when polarization potential decreases to 1.3 V, R_s increases sharply peaking at 6.632 Ω. Then, it goes downward slightly keeping above 6.000 Ω. As polarization potential decrease to 0.9 V, R_s falls severely down to 4.849 Ω and keep steady at 4.800 Ω. The electrolyte resistance R_s is higher than figure before the generation of the SEI-film.

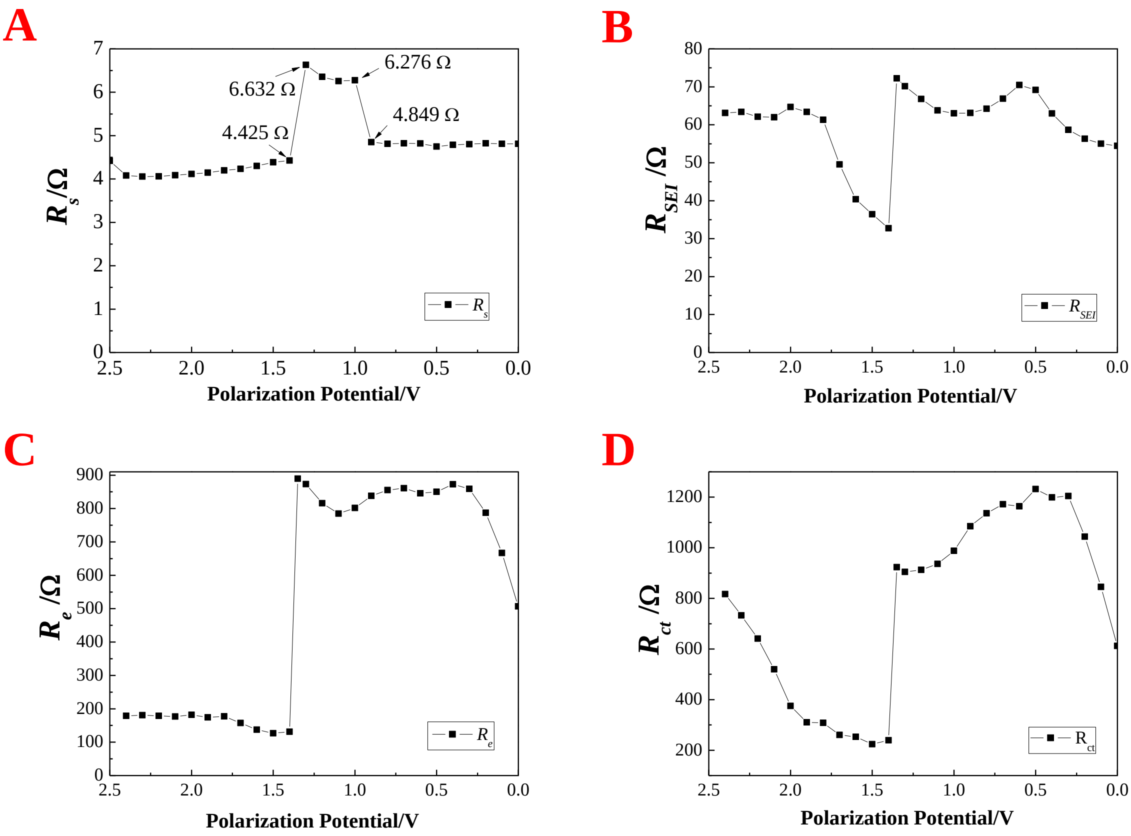

Figure 11. Variations of (A) R_s, (B) R_{SEI}, (C) R_e and (D) R_{ct} with the electrode polarization potentials (vs. Li/Li^+) for $CoSe_2$ in the first discharge process

The main reason could be concluded as follow. When polarization potential decreases to 1.4 V, SEI-film starts to be formed at the interface of anode/electrolyte consuming large amount of ion carriers in a short time resulting in the inhomogeneity of the electrolyte. As a result, diffusion of Li^+ is slowed down, which causes the sharp decrease of conductivity. Then, polarization potential decreases to 0.9 V, SEI-film has been formed completely, and ion carriers in the electrolyte is no longer consumed. The conductivity tends to be steady, however the figure is slightly lower than the initial due to the consumption of ion carriers [48,49].

Fig. 11B, Fig. 11C and Fig. 11D respectively exhibits variations of R_{SEI}, R_e and R_{ct} with the electrode polarization potentials (vs. Li/Li^+) for $CoSe_2$ in the first discharge process. R_{SEI}, R_e and R_{ct} all originally decrease when polarization potential decreases from 2.4 V to 1.4 V. However, during the formation of SEI-film (polarization potential is 1.4-1.3 V) all the figure increased. And the figure of R_e and R_{ct} are much higher than that of R_{SEI}, indicating electron-transfer resistance and charge-transfer resistance make more crucial effect than SEI-film resistance in the lithium intercalation.

4. CONCLUSIONS

Orthorhombic $CoSe_2$ nanoparticles with the size of 100 nm has been synthesized via a facile one-step hydrothermal approach. $CoSe_2$/Li battery and $CoSe_2$@Carbon/Li battery cycled between 2.5 V and 0 V rather than between 3.0V and 0 V both exhibit excellent electrochemical performances. The discharge capacity of $CoSe_2$ exceeds the theoretical value after a few hundred cycles due to the activating reactions and the electric double layer effect. It is confirmed via X-ray diffraction there are two conversion reactions when Li^+ intercalates $CoSe_2$. SEI-film is formed at the interface of anode/electrolyte in the first discharge process consuming large amount of ion carriers when polarization potential decreases from 1.4 V to 0.9 V, which extremely affects electrolyte resistance (R_s). The formation of SEI-film and the accumulation of CoSe, Li_2Se and Co inside electrode cause the irreversible capacity. Nyquist plots of $CoSe_2$ electrode shows electron-transfer resistance (R_e) and charge-transfer resistance (R_{ct}) play more important roles than SEI-film resistance (R_{SEI}) in the first discharge process of lithium intercalation.

ACKNOWLEDGEMENTS
This work would not have been possible without the support from Clean Energy Automotive Engineering Center, School of Automotive Studies of Tongji University. Sincerely we are indebted to the works and reviews done by the previous.

References

1. P. Poizot, S. Laruelle, S. Grugeon, L. Dupont, and J. M. Tarascon, *Nature*, 407 (2000) 496.
2. C. Yuan, H. B. Wu, Y. Xie, and X. W. D. Lou, *Angew. Chem. Int. Ed.*, 53 (2014) 1488.
3. F. M. Courtel, H. Duncan, Y. Abu-Lebdeh and I. J. Davidson, *J. Mater. Chem.*, 21 (2011) 10206.

4. Y. Zhao, X. Li, B. Yan, D. Xiong, D. Li, S. Lawes, and X. Sun, *Advanced Energy Materials*, 6 (2016) 1.
5. A. R. Armstrong, C. Lyness, P. M. Panchmatia, M. S. Islam, and P. G. Bruce, *Nature Materials*, 10 (2011) 223.
6. S. Patoux, L. Daniel, C. Bourbon, H. Lignier, C. Pagano, F. Le Cras, S. Jouanneau, and S. Martinet, *Journal of Power Sources*, 189 (2009) 344.
7. Z. Li, H. Xue, J. Wang, Y. Tang, C. S. Lee, and S. Yang, *ChemElectroChem*, 2 (2015) 1682.
8. L. Mi, H. Sun, Q. Ding, W. Chen, C. Liu, H. Hou, Z. Zheng, and C. Shen, Dalton Trans., 41 (2012) 12595.
9. M. Z. Xue, and Z. W. Fu, *Electrochemistry Communications*, 8 (2006) 1855.
10. Z. Zhang, X. Shi, and X. Yang, *Electrochimica Acta*, 208 (2016) 238.
11. J. Yao, B. Liu, S. Ozden, J. Wu, S. Yang, M. T. F. Rodrigues, K. Kalaga, P. Dong, P. Xiao, Y. Zhang, R. Vajtai, and P. M. Ajayan, *Electrochimica Acta*, 176 (2015) 103.
12. H. Wang, X. Wang, L. Wang, J. Wang, D. Jiang, G. Li, Y. Zhang, H. Zhong, and Y. Jiang, *J. Phys. Chem. C*, 119 (2015) 10197.
13. X. Yang, Z. Zhang, Y. Fu, and Q. Li, *Nanoscale*, 7 (2015) 10198.
14. N. Li, Y. Zhang, H. Zhao, Z. Liu, X. Zhang, and Y. Du, *Inorg. Chem.*, 55 (2016) 2765.
15. M. Z. Xue, and Z. W. Fu, *Solid State Ionics*, 178 (2007) 273.
16. L. Zhang, L. Lu, D. Zhang, W. Hu, N. Wang, B. Xu, Y. Li, and H. Zeng, *Electrochimica Acta*, 209 (2016) 423-429.
17. S. Z. Kang, L. Jia , X. Li, Y. Yin, L. Li, Y. G. Guo, and J. Mu, *Colloids and Surfaces A: Physicochem. Eng. Aspects*, 406 (2012) 1.
18. X. Wang, B. Liu, Q. Xiang, Q. Wang, X. Hou, D. Chen, and G. Shen , *Chemsuchem*, 7 (2013) 308-313.
19. J. Ning, G. Xiao, T. Jiang, L. Wang, Q. Dai, B. Zou, B. Liu, Y. Wei, G. Chen, and G. Zou, *CrystEngComm*, 13 (2011) 4161.
20. D. Wang, K. Zhang, Y. Zhu, Y. Lan, L. Hu, N. Lin, J. Zhou, and Y. Qian, *Materials Letters*, 175 (2016) 32.
21. J. Choi, J. Jin, I. G. Jung, J. M. Kim, H. J. Kim, and S. U. Son, *Chem. Commun.*, 47 (2011) 5241.
22. Z. Zhang, X. Zhao, and J. Li, *Electrochimica Acta*, 176 (2015) 1296.
23. M. Z. Xue, J. Yao, S. C. Cheng, and Z. W. Fu, *Journal of The Electrochemical Society*, 153 (2006) A270.
24. Y. Zhou, J. Mater. Chem. A, 4 (2016) 10906.
25. D. Wei, J. Liang, Y. Zhu, L. Hu, K. Zhang, J. Zhang, Z. Yuan, and Y. Qian, *Electrochemistry Communications*, 38 (2014) 124.
26. M. Z. Xue, and Z. W. Fu, *Acta Chimica Sinica*, 65 (2007) 2715.
27. X. Wang, K. Cai, and S. Chen, *Journal of Nanoscience and Nanotechnology*, 13 (2013) 1106.
28. M. Z. Xue, and Z. W. Fu, *Journal of Alloys and Compounds*, 458 (2008) 351.
29. H. T. Kwon, and C. M. Park, *Journal of Power Sources*, 251 (2014) 319.
30. Z. Zhang, Y. Fu, X. Yang, Y. Qu, and Q. Li, *Electrochimica Acta*, 168 (2015) 285.
31. Y. Fu, Z. Zhang, K. Du, Y. Qu, Q. Li, and X. Yang, *Materials Letters*, 146 (2015), 96.
32. J. J. Ding, Y. N. Zhou, Y. H. Cui, and Z. W. Fu, *ECS Electrochemistry Letters*, 1 (2012) A7.
33. J. H. Jeong, D. W. Jung, and E. S. Oh, Journal of Alloys and Compounds, 613 (2014) 42.
34. H. Xu, G. Chen, R. Jin, D. Chen, Y. Wang, and J. Pei, RSC Adv., 4 (2014) 8922.
35. H. Xu, G. Chen, R. Jin, J. Pei, and Y. Wang, CrystEngComm, 15 (2013) 1618.
36. J. Bludskά, I. Jakubec, S. Karamazov, J. Horάk, and C. Uher, *Journal of Solid State Chemistry*, 183 (2010) 2813.
37. W. Zhang, Z. Yang, J. Liu, Z. Hui, W. Yu, Y. Qian, G. Zhou, and L. Yang, *Materials Research Bulletin*, 35 (2000) 2403.
38. J. Yang, X. Shen, Z. Ji, and G. Zhu, *J Mater Sci*, 48 (2013) 7913.

39. H. Sun, L. Zhang, Z. S. Wang, and *J. Mater. Chem. A*, 2 (2014) 16023.
40. Q. Liu, J. Shi, J. Hu, A. M. Asiri, Y. Luo, and X. Sun, *ACS Appl. Mater. Interfaces*, 7 (2015) 3877.
41. J. Yang, G. H. Cheng, J. H. Zeng, S. H. Yu, X. M. Liu, and Y. T. Qian, *Chem. Mater*, 13 (2001) 848.
42. M. R. Gao, W. T. Yao, H. B. Yao, and S. H. Yu, *J. AM. CHEM. SOC*, 131 (2009) 7486-7487.
43. J. Maier, *Nature Materials*, 4 (2005) 805.
44. J. Jamnik, and J. Maier, *Phys. Chem. Chem. Phys.*, 5 (2003) 5215.
45. K. Zhang, Z. Hu, X. Liu, Z. Tao, and J. Chen, *Adv. Mater.*, 27 (2015) 3305.
46. W. Wei, S. Yang , H. Zhou , I. Lieberwirth , X. Feng , and K. Müllen, *Adv. Mater.*, 25 (2013) 2909.
47. Y. Sun, X. Hu, W. Luo, F. Xia, and Y. Huang, *Adv. Funct. Mater.*, 23 (2013) 2436.
48. P.L. Moss, G. Au, E.J. Plichta, and J.P. Zheng, *Journal of Power Sources*, 189 (2009) 66.
49. M. Itagaki, S. Yotsuda, N. Kobari, K. Watanabe, S. Kinoshita, and M. Ue, *Electrochimica Acta*, 51 (2006) 1629.